Saturn's inner magnetospheric convection pattern: Further evidence

M. F. Thomsen,[1] E. Roussos,[2] M. Andriopoulou,[2,3] P. Kollmann,[2,3] C. S. Arridge,[4] C. P. Paranicas,[5] D. A. Gurnett,[6] R. L. Powell,[1,7] R. L. Tokar,[1] and D. T. Young[8]

Received 29 December 2011; revised 7 June 2012; accepted 17 July 2012; published 12 September 2012.

[1] Observations of the radial locations of satellite absorption microsignatures in energetic particle data at Saturn have suggested the existence of an average convection pattern, fixed in local time, that is superimposed on the dominant near-corotation of the inner magnetosphere. Such a pattern should have additional observational consequences, and we use several different Cassini data sets to test these expectations. These include day/night asymmetries in the A-ring absorption signature of high-energy particles and total electron density, day/night asymmetries in plasma ion and electron temperatures, and day/night asymmetries in energetic-particle phase-space densities. For L > 4, the observations are found to be consistent with expectations based on the suggested convective drifts in a global noon-to-midnight electric field, such that particles drift outward on the dawn side of the magnetosphere and inward on the dusk side, resulting in drift orbits with an outward offset toward noon. The different data sets yield similar estimates of the required radial offsets, ∼0.5–1 Rs in the region inside L = 10. The corresponding convection electric field appears to decrease with increasing radial distance, from ∼0.3 mV/m near Tethys to ∼0.1 mV/m beyond Dione. The source of such an electric field remains a puzzle, but whatever the source, it appears to be a dominant factor in the circulation of plasma in Saturn's inner magnetosphere. For L < 4, the observations are not fully consistent with such a global convection field, and other explanations for A-ring absorption asymmetries are needed.

Citation: Thomsen, M. F., E. Roussos, M. Andriopoulou, P. Kollmann, C. S. Arridge, C. P. Paranicas, D. A. Gurnett, R. L. Powell, R. L. Tokar, and D. T. Young (2012), Saturn's inner magnetospheric convection pattern: Further evidence, *J. Geophys. Res.*, *117*, A09208, doi:10.1029/2011JA017482.

1. Introduction

[2] The field of comparative magnetospheres involves the identification and quantitative understanding of plasma sources, transport mechanisms, acceleration processes, and loss processes, including the dynamical interplay of all of these. With the arrival of the Cassini spacecraft at Saturn in 2004, our understanding of all of these aspects of Saturn's magnetosphere has grown enormously. We now know that Saturn's icy satellite Enceladus is the primary source of plasma for the inner magnetosphere [e.g., *Hansen et al.*, 2006; *Waite et al.*, 2006; *Sittler et al.*, 2008] and that the dominant transport is azimuthal circulation around the planet [e.g., *Richardson*, 1986; *Thomsen et al.*, 2010], forced by electrodynamic coupling to the rapidly rotating ionosphere [e.g., *Hill*, 1979]. (In this paper, we use the term "inner magnetosphere" to refer to the largely dipolar region inside of a dipole L value of ∼10.) In the radial direction, dynamical processes driven by the planet's rapid rotation, such as flux tube interchange [e.g., *Burch et al.*, 2005; *Hill et al.*, 2005] and tail plasmoid production [e.g., *Jackman et al.*, 2007; *Hill et al.*, 2008], transport plasma produced in the inner magnetosphere outward to down-tail loss. These rotation-driven processes are primarily dominant only beyond a dipole L-value of ∼6–8 [e.g., *Sittler et al.*, 2008; *Chen et al.*, 2010]. Inside of that approximate distance, the plasma appears to be stable against interchange, and radial plasma transport is slower and dependent on other processes, such as diffusion.

[3] The nature and rate of radial transport in the inner magnetosphere has important implications for determining

[1]Los Alamos National Laboratory, Los Alamos, New Mexico, USA.
[2]Max Planck Institute for Solar System Research, Katlenburg-Lindau, Germany.
[3]Institute for Geophysics and Extraterrestrial Physics, Technical University of Braunschweig, Braunschweig, Germany.
[4]Mullard Space Science Laboratory, University College London, Holmbury-St. Mary, UK.
[5]Applied Physics Laboratory, Johns Hopkins University, Laurel, Maryland, USA.
[6]Department of Physics and Astronomy, University of Iowa, Iowa City, Iowa, USA.
[7]Institute of Geophysics and Planetary Physics, University of California, Los Angeles, California, USA.
[8]Southwest Research Institute, San Antonio, Texas, USA.

Corresponding author: M. F. Thomsen, MS D466, Los Alamos National Laboratory, Los Alamos, NM 87545, USA. (mthomsen@lanl.gov)

0148-0227/12/2011JA017482

the plasma source strength, for understanding radiation belt formation and evolution, and for quantifying the interactions between charged particles and neutral materials. Hence, it has been one of the objectives of the Cassini mission to determine the nature and strength of radial transport processes, and a number of different approaches have been employed.

[4] The primary radial transport in the inner magnetosphere of Saturn has long been attributed to radial diffusion, driven by electric and magnetic field fluctuations arising from solar wind variability and/or upper atmospheric winds. One of the most powerful techniques for determining the strength of the diffusion has been the analysis of "microsignatures" in energetic particle fluxes, which arise from the absorption of charged particles as they drift past planetary satellites [*Paranicas et al.*, 2005; *Roussos et al.*, 2007]. The values of the radial diffusion coefficient derived from individual microsignatures vary by an order of magnitude at each satellite, suggesting significant temporal variability in the fluctuating field amplitudes. These analyses found long diffusion times, so that individual particles are likely to encounter a given satellite at least once during their diffusive transport, implying the satellites should provide an effective barrier to the radial transport of charged particles.

[5] Based on CAPS electron observations in the inner magnetosphere, *Rymer et al.* [2007] argued that typical radial transport times in the inner magnetosphere probably exceed ~150 h, which is the time required for temperature equilibration between cold electrons and warmer protons, as suggested by the fact that the observed cool electron temperature tracks the proton temperature rather well [e.g., *Sittler et al.*, 2006]. This requires that average radial transport speeds be less than ~1 Rs/150 h ~0.1 km/s. The slow radial diffusion derived from microsignature analysis could easily meet this upper limit criterion.

[6] Cassini has also provided some direct measurements of the instantaneous transport. Using plasma data from the Cassini Plasma Spectrometer (CAPS), *Sittler et al.* [2006] and *Wilson et al.* [2008] derived radial flow velocities that were variable (both positive and negative), ranging from ~0 km/s at L = 4 to ~10 km/s at L = 10.

[7] The above observations pertain to fluctuating, i.e., diffusive transport. However, there have also been several reports suggesting the existence of more coherent, global modes of radial transport in Saturn's inner magnetosphere. *Gurnett et al.* [2007] found that the total electron density in the inner magnetosphere ($3 < L < 5$) varies sinusoidally with longitude in the corotating frame of reference. They interpreted this as evidence for a corotating convection pattern in which plasma flows outward in the denser sector and inward in the less-dense sector. The convection was attributed to an $m = 1$ centrifugally driven instability caused by the difference in the centrifugal force in the denser vs. less-dense sectors. In an independent analysis, *Goldreich and Farmer* [2007] proposed a similar corotating convection pattern to explain observed periodicities in the magnetic field components.

[8] In addition to a possible corotating convection pattern, there have been several observations that imply the existence of a large-scale convection pattern that is fixed in local time. Based on inbound/outbound asymmetries in energetic electron fluxes seen at 6–15 Rs with the Pioneer and Voyager flybys, *Cooper et al.* [1998] suggested that penetration of the solar wind electric field into Saturn's magnetosphere, analogous to the case at Earth, could create "banana-shaped" drift orbits that don't encircle the planet for energies where the azimuthal gradient and curvature drift speed is near but opposite in direction to the corotational drift speed. The required penetration field would be in the dusk-to-dawn direction.

[9] With the arrival of Cassini at Saturn, new observations pointed toward the existence of local-time-fixed, large-scale convection in the inner magnetosphere. Early observations of satellite absorption microsignatures [*Roussos et al.*, 2005; *Paranicas et al.*, 2005] showed that they are frequently displaced in the radial direction from the absorbing satellite's known orbit, suggesting non-circular drift orbits that would be inconsistent with pure gradient-curvature and corotation drift in the highly symmetric magnetic field of the inner magnetosphere. Further, these radial offsets were found to be largely outward from the satellite orbit on the dayside and inward of it on the night side, implying a noncircularity to the drift paths that is roughly fixed in local time [*Roussos et al.*, 2005, 2007]. The local time dependence of the offsets would require a global noon-to-midnight electric field of magnitude >0.1 mV/m [*Roussos et al.*, 2007], which is substantially larger than the value of 0.02 mV/m estimated by *Cooper et al.* [1998] for solar wind-driven convection. Moreover the orientation of the required electric field (noon-to-midnight) is 90 degrees away from what would be expected from solar wind driving. Subsequent analysis of a much larger set of absorption microsignatures [*Andriopoulou et al.*, 2012] has confirmed the basic local-time pattern of radial offsets, and based on the age of the observed signatures, has estimated that the required strength of the (assumed uniform) noon-to-midnight electric field lies in the range 0.01–1.0 mV/m, for microsignatures of both Tethys (L = 4.9) and Dione (L = 6.2), with the most probable value around 0.15 mV/m.

[10] Other evidence pointing to a systematic noncircularity of inner-magnetospheric charged-particle drift orbits was presented by *Paranicas et al.* [2010], who pointed to a day/night asymmetry in the distance at which energetic particles begin to show the effects of absorption by the particles of the A-ring. They found that during Saturn Orbit Insertion, as Cassini passed over the outer edge of the A-ring, the absorption signature was seen very near the ring edge during the outbound pass at 23.2 LT but was seen ~0.09 Rs further out during the inbound pass at 12.5 LT. They concluded that the corresponding charged-particle drift paths must be shifted toward noon, requiring a noon-to-midnight electric field ~0.5 mV/m at L~2.4.

[11] The existence of such a global circulation pattern in the inner magnetosphere of Saturn should produce other potentially observable signatures. The purpose of the present study is to identify what those signatures might be and then to use Cassini observations to test those expectations. We find that a number of these tests support the conclusion that there exists a local-time-fixed convection pattern in Saturn's inner magnetosphere, with relatively consistent estimates for the typical day-night radial drift offsets over a wide range of energies, yielding estimates of the noon-to-midnight electric field that are consistent with those reported in the above mentioned studies. However, the observational evidence from the innermost magnetosphere (L~3) is not fully consistent with the expectations for circulation in a noon-to-

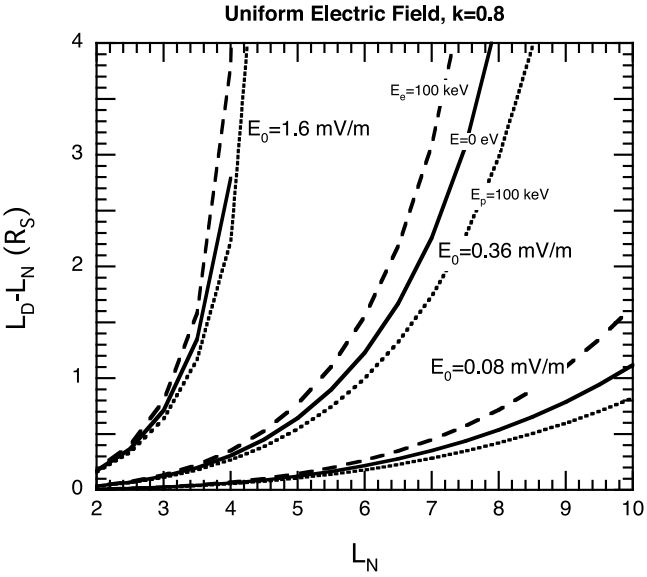

Figure 1. Day-night radial drift offsets that would arise for ions and electrons with energies of zero and 100 keV for three different values of the convection electric field strength.

midnight electric field, and we conclude that in that region the previously identified A-ring absorption asymmetry may be due to other causes.

2. Predicted Signatures of Noon-to-Midnight Global Electric Field

[12] A noon-to-midnight global electric field would introduce a dawnward component of E × B drift within the inner magnetosphere. Combined with the dominant corotational motion, this dawnward drift would lead to a radial offset in otherwise circular charged-particle drift orbits. In drifting from midnight to noon, a particle whose net azimuthal drift (corotation + convection + gradient/curvature) is eastward would tend to drift radially outward during the dawn side of its orbit and inward during the dusk portion. Thus, the maximum radial extent of the orbit would be at noon local time, and the minimum would be at midnight. By contrast, a particle whose net azimuthal drift is westward would drift inward as it moved from midnight toward noon and outward as it returned to midnight. For such particles, which at Saturn are very high-energy electrons whose westward gradient/curvature drift can overwhelm the rapid eastward corotation, the radial extent of the orbit would be a minimum at noon and a maximum at midnight.

[13] The magnitude of the day-night orbital offset can be calculated as a function of the assumed global convection strength, species, and energy. For a uniform noon-to-midnight field, particle drift orbits may be described by the following equation:

$$\frac{dL}{d\varphi} = \frac{(cE_0/B_0R_S)L^3\sin\varphi}{k\Omega_S + \omega_D + (cE_0/B_0R_S)L^2\cos\varphi} \quad (1)$$

where φ is the local time, E_0 is the strength of the uniform convection electric field, B_0 is Saturn's dipole surface field strength, Ω_S is the full corotational angular velocity, k is the fraction of corotation at which the plasma actually flows, and ω_D is the gradient/curvature drift velocity of the particle in the corotating frame [e.g., *Thomsen and Van Allen*, 1980, equation (2)]. For a corotational fraction of k = 0.8 [e.g., *Wilson et al.*, 2008], Figure 1 shows the day-night offsets that would result from a set of E_0 values roughly spanning the range derived by *Andriopoulou et al.* [2012]. Note that the offsets expected for electrons (dashed curves) are larger than those for protons with the same energy (dotted curves) because the gradient/curvature drift of electrons is opposite to the corotation direction, leading to a slower net azimuthal drift, exposing the electrons to the radial drift for a longer time.

[14] The outward displacement of drift orbits from midnight to noon should produce at least three potentially observable consequences:

[15] 1) Satellite microsignatures encountered on the dayside of the magnetosphere should tend to be observed at or beyond the responsible satellite's orbit, whereas those encountered on the nightside should tend to be observed at or inside the satellite orbit, as indeed is the case [*Roussos et al.*, 2005; *Paranicas et al.*, 2005; *Andriopoulou et al.*, 2012].

[16] 2) The sharp cutoff in the radial profile of trapped charged particles caused by the strong losses due to absorption by A-ring material should be displaced outward from the A-ring boundary itself on the dayside, as reported by *Paranicas et al.* [2010]. A similar day-night asymmetry in the location of the absorption boundary should exist for other populations than those reported by *Paranicas et al.* [2010]. Moreover, the direction of the day-night offset should reverse for very high-energy electrons, whose net drift is westward.

[17] 3) Because the azimuthal drift period of charged particles (~10 h) is short compared to source, loss, and energization timescales [e.g., *Sittler et al.*, 2008], we would expect the transport from night to day and back again to be largely adiabatic. Thus, particles moving outward would progressively lose energy as they drift toward lower magnetic field strengths at larger radial distances and reverse the trend as they return to larger field strengths at lower radial distances. This adiabatic effect is expected both for the thermal plasma (ions and electrons) and for energetic particles.

[18] In the following, we examine Cassini observations bearing on these three expected consequences of a noon-to-midnight electric field. This will be a quantitative test as well as a qualitative one, with the figure of merit being whether or not the observations yield day-night radial offsets consistent with those seen in the microsignature displacements.

2.1. Microsignature Displacements

[19] As discussed above, the tendency for satellite absorption microsignatures to be displaced outward from the satellite orbit on the dayside and inward from it on the night side is one of the strongest pieces of evidence pointing to a systematic drift pattern in the inner magnetosphere. Figure 2, adapted from *Andriopoulou et al.* [2012], illustrates this effect for a large set of identified microsignatures associated with Tethys. As discussed by *Andriopoulou et al.* [2012], the maximum radial offsets that could be produced by asymmetries in the magnetic field are very much smaller than these observed offsets, so the general trend in Figure 2 requires a non-circular electric drift. From Figure 2, the maximum dayside displacement of Tethys' microsignatures is in the

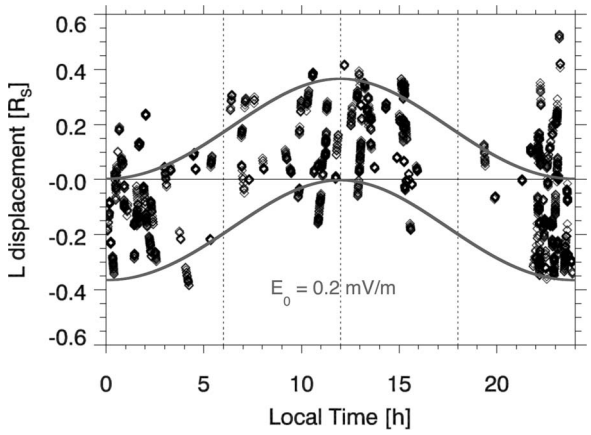

Figure 2. Radial offsets of charged-particle absorption microsignatures of Tethys, shown as a function of the local time of observation. The offsets are measured from the nominal circular orbit of the satellite itself. There is a clear tendency for microsignatures observed on the dayside to be displaced outward relative to the satellite orbit, while microsignatures observed on the night-side tend to be displaced inward relative to the satellite orbit. The solid curves show the envelope of displacements that could result from a uniform noon-to-midnight electric field of magnitude 0.2 mV/m. Adapted from *Andriopoulou et al.* [2012].

neighborhood of +0.4 Rs, and the maximum nightside displacement is near −0.4 Rs. Smaller displacements are also seen, including some with the opposite sign, but for the most part these are within the band of expected displacements for signatures created and observed at a variety of local times [e.g., *Andriopoulou et al.*, 2012, Figure 9]. The solid lines in Figure 2 show the envelope of displacements that could result from a uniform noon-to-midnight electric field of magnitude 0.2 mV/m, the most probable value found by *Andriopoulou et al.* [2012]. For Dione, the maximum dayside and nightside displacements are ∼0.8 Rs [*Andriopoulou et al.*, 2012].

2.2. A-Ring Total Electron Absorption Asymmetry

[20] The day/night asymmetry in the A-ring absorption signature for energetic particles noted by *Paranicas et al.* [2010] should also be found in the total electron density profile, determined from measurements by the Cassini/RPWS instrument (Radio and Plasma Wave Science) [*Gurnett et al.*, 2004]. Figure 3, adapted from *Gurnett et al.* [2005], shows the inferred total electron density for Cassini's closest approach to Saturn during the orbit insertion maneuver in 2004. The spacecraft crossed the outer edge of the A-Ring (L = 2.269) [*Spitale and Porco*, 2009] at a local time of 12.5 LT on the inbound leg and at a local time of 23.2 LT on the outbound leg. As noted previously by *Gurnett et al.* [2005], the total electron density drops sharply at the A-ring, as magnetospheric electrons are absorbed by the ring material. From Figure 3, it is apparent that during the outbound (night-side) crossing, the sharp drop in electron density is essentially coincident with the L shell of the outer edge of the A-ring. By contrast, during the inbound (dayside) crossing, the sharp drop in electron density occurs ∼11 min earlier than the traversal of the L shell of the outer edge of the A-ring. Thus, the A-ring absorption edge is displaced ∼0.17 Rs outward near noon compared to where it occurs near midnight. This is of the same order as the 0.09 Rs offset reported by *Paranicas et al.* [2010] and is consistent with non-circular particle drift orbits that are slightly further from the planet on the dayside than on the night-side. Since the total electron density is dominated by

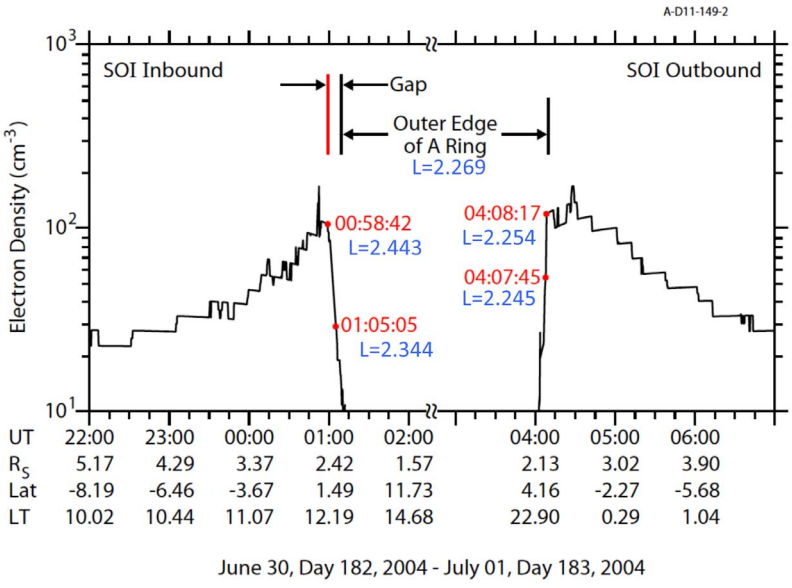

Figure 3. Total electron density inferred from measurements of the RPWS during Saturn Orbit Insertion (SOI) in 2004. The interval includes the periapsis of the pass and shows the inbound and outbound crossings of the L-shell of the outer edge of the A-ring, which occurred at local times of 12.5 and 23.2, respectively. From *Gurnett et al.* [2005]. Reprinted with permission from AAAS.

very-low-energy electrons, these drift orbits are totally attributable to electric field drifts (corotation plus convection). To produce an outward displacement at noon relative to midnight, a noon-to-midnight convection electric field would be necessary.

2.3. A-Ring Energetic Electron Absorption Asymmetry

[21] The observations presented by *Paranicas et al.* [2010] at the A-ring crossing corresponded to particle species/energies for which the net azimuthal drift was eastward, for which an outward displacement on the dayside is expected. However, the LEMMS channel E7, which probably counts electrons with energies >5 MeV, was reported to show the same inbound/outbound offset as the lower-energy channels [*Paranicas et al.*, 2010]. If the drift asymmetries are due to a noon-to-midnight electric field, this offset is actually contrary to the expectations for such high-energy electrons, which should have a net westward drift [c.f., *Roussos et al.*, 2007], leading to an inward displacement on the dayside relative to the night-side location, as discussed above. Thus, the evidence from the day-night asymmetry in the location of the A-ring absorption boundary for high-energy electrons is apparently not consistent with the presence of a net noon-to-midnight electric field near the A-ring.

2.4. Plasma Ion Temperature Asymmetry

[22] If the transport of the plasma is effectively adiabatic over the corotation timescale, a day-night asymmetry in the drift orbits should produce an adiabatic cooling and heating as the plasma convects from the night-side to the dayside and back again. The overall radial temperature profiles, increasing as they do with increasing radial distance, are clearly not adiabatic [*Rymer et al.*, 2007; *Thomsen et al.*, 2010], but assuming that the temperatures behave roughly adiabatically over the short time to corotate around the planet, we would expect that over one drift orbit the perpendicular temperature $T_\perp \sim B$, the magnetic field strength. Since the plasma temperature is dominated by $T_\perp$ [e.g., *Wilson et al.*, 2008], we can make the approximation that $T \sim B$, so that, in the nearly dipolar field of the inner magnetosphere, T along drift orbits should vary $\sim 1/L^3$. Thus, a parcel of plasma that on the nightside had a temperature T_N at a radial distance L_N, would have a temperature of $T_D = T_N \cdot (L_N/L_D)^3$ if it drifted to a radial distance L_D on the dayside. The radial distributions of plasma ion parameters (e.g., density, temperature, velocity) within Saturn's magnetosphere have previously been explored based on measurements from the Cassini Plasma Spectrometer/Ion Mass Spectrometer (CAPS/IMS) sensor [*Young et al.*, 2004; *Wilson et al.*, 2008; *Thomsen et al.*, 2010]. In Figure 4, with the same set of numerical moments used by *Thomsen et al.* [2010], we examine the local time dependence of the derived temperatures of the three major ion species in Saturn's magnetosphere (H^+, H_2^+, and W^+, where "W^+" represents the set of water-group ions, O^+, OH^+, H_2O^+, and H_3O^+). Because of the strong radial dependence of these parameters [*Wilson et al.*, 2008; *Thomsen et al.*, 2010], the data have been binned into L-ranges of 1 Rs in width. The data in Figure 4 have been subjected to the same set of filters discussed by *Thomsen et al.* [2010]: 1) The CAPS actuator was operating, 2) the spacecraft was not rolling, 3) the corotation direction was in the field of view, and 4) the spacecraft latitude was between −5 and +5 degrees. The solid dots show individual 7-min measurements, and the boxes show the median values in 2-h local time bins.

[23] While there is clearly a large amount of scatter in the individual measurements, it is apparent from essentially all the panels in Figure 4 that there is a local-time dependence to the temperatures of all three major ion species within Saturn's inner magnetosphere. The general trend is for the temperatures to be highest on the night-side and lowest near noon, with a fairly continuous transition between the two. Figure 5 emphasizes this contrast by comparing the radial distribution of temperatures measured between 9 and 15 LT ("dayside," left) and between 21 and 3 LT ("nightside," right). The solid lines in each panel show power law fits to the night-side temperature profile of each species ($T = aL^b$), and the dashed lines show the corresponding fits to the dayside profile. Not only is there a clear and consistent offset between the night-side and dayside fits, but it is also obvious that most of the dayside individual measurements lie below the night-side fit, while most of those on the night-side lie well above the dayside fit, confirming the average day/night asymmetry revealed by the fits. The clearly apparent offset between the dayside and nightside temperatures has also been formally confirmed with a Kolmogorov-Smirnov test of the difference between two distributions [e.g., *Press et al.*, 2001, chapter 14.3]: With the data sorted in 0.5-Rs bins, the probability is at best (11, 1.7, 2.9) percent that the measured dayside and nightside temperatures of (H^+, H_2^+, W^+) in the radial bin 5.0–5.5 Rs could have been drawn from the same distribution. For all other radial bins between 5 and 10 Rs, the probabilities are negligible ($\ll 10^{-3}$) for all three species.

[24] Thus, the plasma ion temperatures qualitatively exhibit the day-night asymmetry we would expect for non-circular drift orbits that extend further from Saturn on the dayside than on the nightside. We can also assess quantitatively the day-night drift offset that would be needed to produce the asymmetry seen in Figures 4 and 5. Figure 6 shows the day and night measurements from Figure 5, averaged in 0.5-Rs bins. The error bars shown in the left-hand panels are the standard deviations about the means; they are rather large, as expected from Figure 6, but the estimated standard error in these means is only ∼1/6 as large, indicating that the calculated means are good estimations of the true means. As already argued above, the standard deviations in Figure 6 show that the two data sets (day and night) are significantly displaced relative to one another for all three species. The dashed curves plotted in Figure 6 are fits to the function

$$\log\langle T_i \rangle = A(\log L)^2 + B(\log L) + C \qquad (2)$$

which is simple to use and reasonably well represents the radial dependence of the mean temperatures. The error bars shown in the right-hand panels are the RMS deviations between these fits and the means. Table 1 gives the values of the derived fit coefficients in equation (2) for each species for dayside ($9 < \mathrm{LT} < 15$) and night-side ($21 < \mathrm{LT} < 3$) measurements.

[25] With the dayside and night-side bin-averaged temperatures represented by equation (2), the adiabatic requirement that $T_D L_D^3 = T_N L_N^3$ allows us to determine the dayside

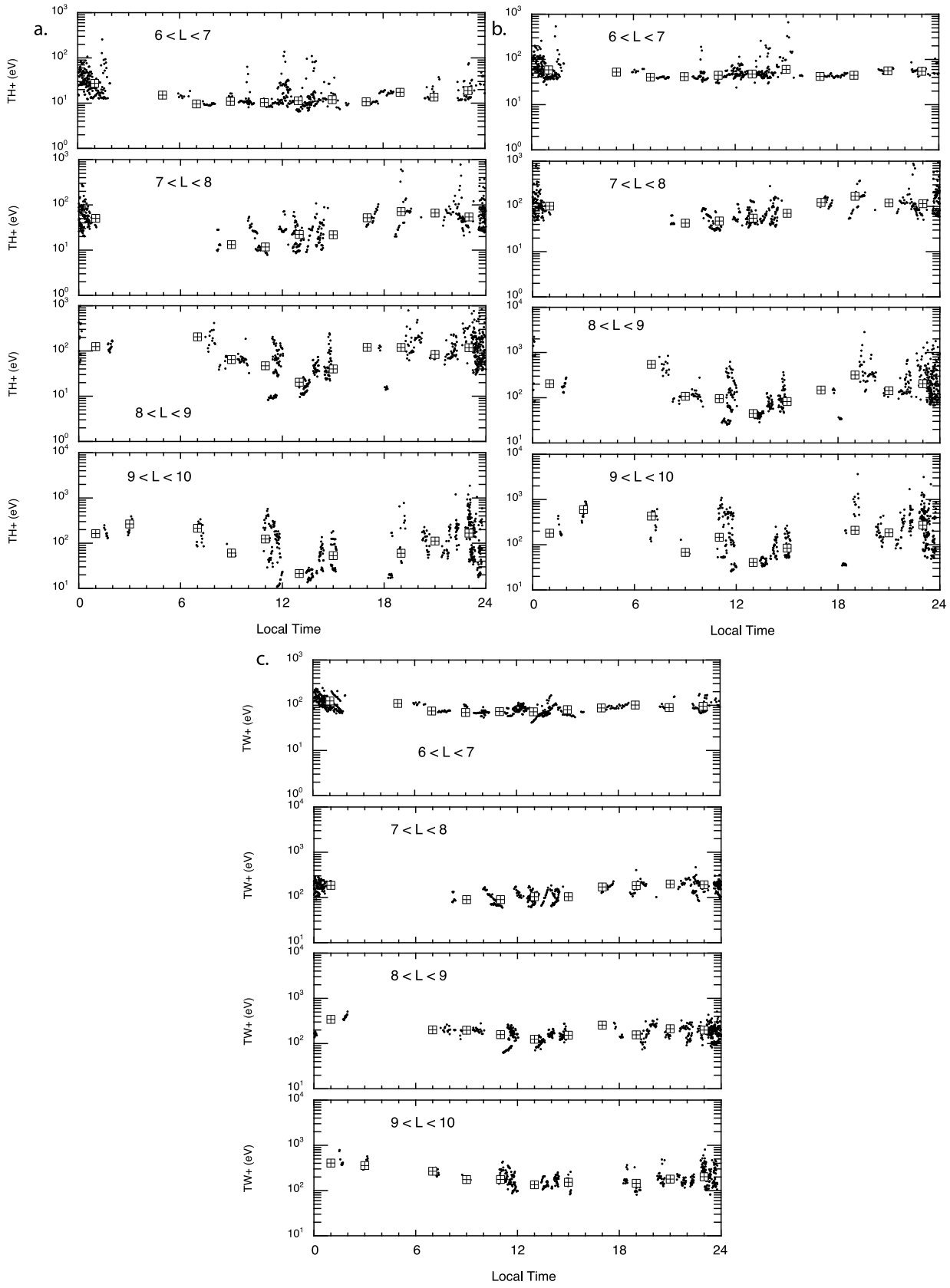

Figure 4. (a) Local time dependence of the H^+ ion temperature derived from CAPS IMS measurements, for different 1-Rs L bins between L = 6 and L = 10. Solid dots indicate individual 7-min measurements, and boxes indicate the median values in 2-h local time bins. (b) Same as Figure 4a for H_2^+ ions. (c) Same as Figure 4a for W^+ ions.

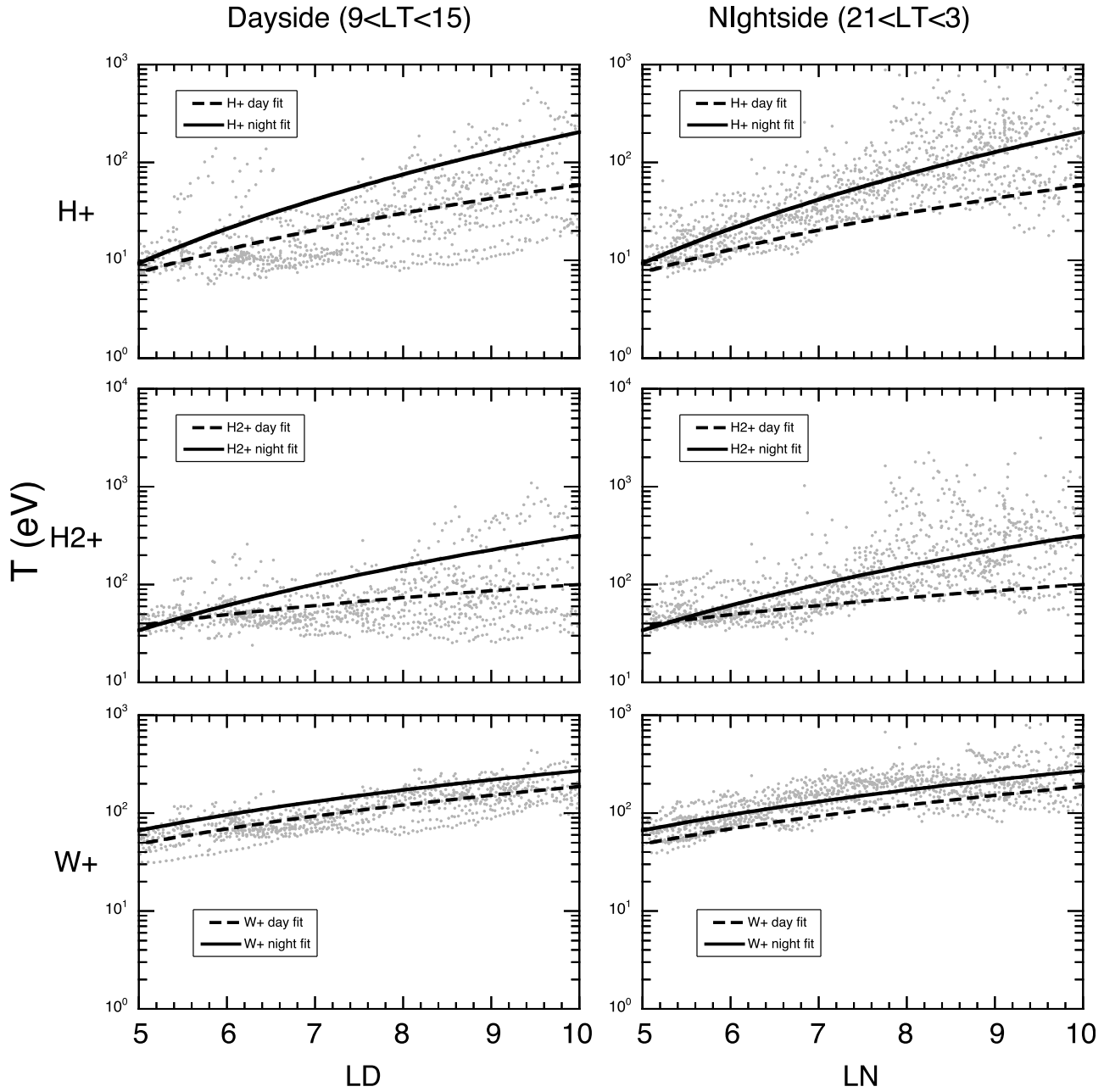

Figure 5. (left) Dayside (9 < LT < 15 h) and (right) nightside (21 < LT < 3 h) ion temperature profiles for the three major plasma species. Grey dots show individual 7-min measurements, solid curves are the nightside power law fits, and dashed curves are the dayside power law fits.

L value that would adiabatically map to a given nightside L value:

$$\log(L_D) = \frac{-(B_D+3) + \sqrt{(B_D+3)^2 - 4A_D(C_D - F_N)}}{2A_D} \quad (3)$$

where

$$F_N = A_N(\log L_N)^2 + B_N(\log L_N) + C_N$$

Figure 7 shows the radial offsets $(L_D\text{-}L_N)$ that would result from adiabatic mapping of the profiles given by the fit parameters in Table 1. The curves only extend over the range of L_N for which the derived L_D is within the range of validity of the fit to equation (2) (i.e., $5 < L_D < 10$). To estimate the uncertainties in these derived offsets, we use equation (3) to map the maximum and minimum ranges

$$\max[\log T_N] \rightarrow \min[\log T_D] \quad (4a)$$

$$\min[\log T_N] \rightarrow \max[\log T_D] \quad (4b)$$

so that equation (4a) produces the maximum offset for a given L_N, and equation (4b) produces the minimum offset.

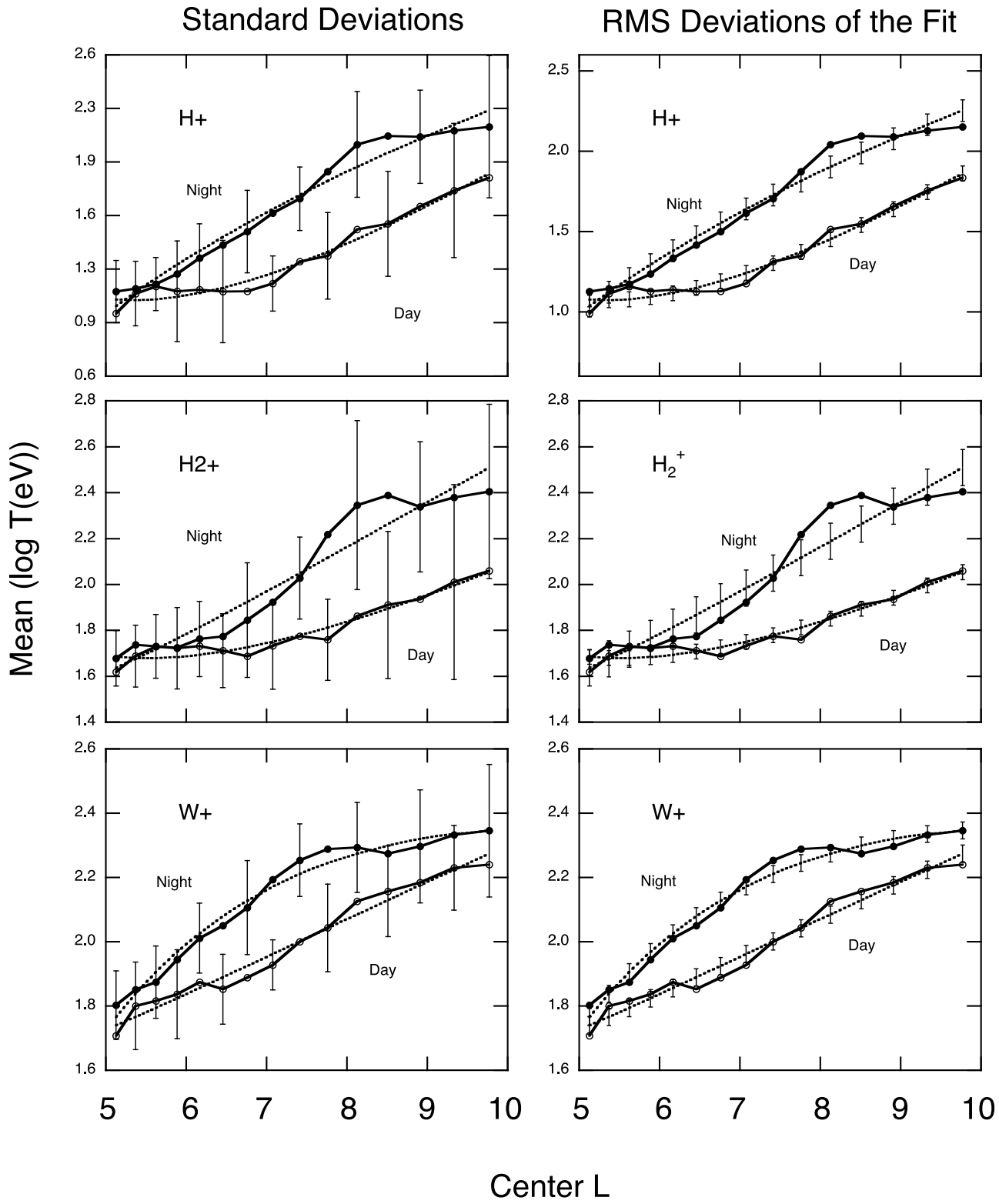

Figure 6. Mean nightside (21 < LT < 3) and dayside (9 < LT < 15) ion temperatures in 0.5-Rs bins. Error bars in the left-hand panels show the standard deviations about the mean, while the error bars in the right-hand panels show the RMS deviations between the means and the analytical fits to equation (2) (dotted lines in both panels).

Table 1. Parameters for Fits of Equation (2) to Radial Dependence of Ion Temperatures (in eV)

Species	A_N	B_N	C_N	A_D	B_D	C_D
H^+	0.19315	4.0170	−1.9129	11.573	−16.872	7.2226
H_2^+	4.5086	−4.5481	2.5932	6.0689	−8.9995	5.0149
W^+	−5.8957	12.094	−3.8486	2.2943	−1.9928	1.9981

Here, to estimate max (min) [logT] we take the fits to equation (2) given by the coefficients in Table 1 and add (subtract) the RMS deviations between the fits and the means shown in the right-hand panels of Figure 6. We believe that the true uncertainties in the estimated offsets in Figure 7 are probably slightly larger than this (e.g., we have not included the contribution from the standard error in the means). Further, while the mean temperatures in Figure 6 are well-determined, we also believe that those for the light ions (H^+ and H_2^+) are probably somewhat "contaminated" by the episodic presence of hotter populations that are delivered from the outer magnetosphere to the inner magnetosphere during interchange events. These hot populations, which appear primarily outside of L∼6–7 and can be seen by the large scatter of higher-T points in the upper two panels of Figure 5, are typically dominated by light ions, so the W^+ is not particularly affected. Hence in using the quantitative estimates of the required day-night offset, the results in Figure 7 from the water-group ions are to be preferred.

[26] In summary, while there is significant scatter in the individual measured ion temperatures (Figures 4 and 5), the evidence is clear that there is a net day-night difference in the average temperatures (Figure 6), consistent with expectations based on a global noon-to-midnight electric field. With perhaps a factor of 2 uncertainty, the average necessary day-night offsets are in the neighborhood of a few tenths of an Rs (Figure 7).

2.5. Plasma Electron Temperature Asymmetry

[27] Exactly analogous to the discussion for plasma ions above, a similar expectation exists for day-night temperature differences in the plasma electrons. Figure 8, in a format similar to Figure 4, shows that the plasma electrons in Saturn's inner magnetosphere exhibit the same sort of day/night asymmetry seen in the ions [see also *DeJong et al.*, 2011]. The temperatures perpendicular to the magnetic field have been derived by numerical integration of the fluxes in the lower-energy (<150 eV) part of the spectrum observed by the CAPS/ELS instrument (Electron Spectrometer) [*Young et al.*, 2004; *Lewis et al.*, 2008]. Each value represents a summation over half a CAPS actuator cycle (∼3.5 min). Only those spectra are used where the spacecraft potential is clearly determined, to ensure that the full distribution is observed. The uncertainty in the derived temperatures is ∼25–50% [*Arridge et al.*, 2009]. In Figure 8, the individual measurements are shown as solid dots, and the boxes show the median and 25th/75th percentile values in 2-h LT bins. The vertical bars show the range of values in each 2-h bin. For all the radial ranges in Figure 8, the maximum temperature lies near local midnight, with the minimum similarly near noon.

[28] Figure 9 is analogous to Figure 5, showing the dayside and night-side cold electron temperatures versus L. For these cold electrons, we have empirically fit the radial dependence with a hyperbolic tangent:

$$T_{ce} = a_0 + a_1 \tanh\left(\frac{L - a_2}{a_3}\right) \quad (5)$$

The day and night fit parameters are given in Table 2, and Figure 9 shows the resulting curves for the night-side (solid) and dayside (dashed) sets of data. Unlike the fits used for the ions, the tanh fit does not yield a nice analytical expression for the offset analogous to equation (3). We can, however, solve for the offset by adiabatically mapping a number of points on the night-side temperature curve to various dayside radial distances and interpolating the points of intersection with the dayside temperature curve. Figure 10a shows this mapping, and Figure 10b shows the resulting night-to-day displacements. The gray shading in Figure 10b shows the range of offsets determined in analogy to equations (4a) and (4b) above, with the min and max T values based on the uncertainties in the fits (Figures 9 and 10a). As with the ions, Figure 10 shows that the inner magnetospheric electron temperatures are consistent with day-night drift offsets ∼several tenths of an Rs.

2.6. Energetic Particle Flux Asymmetry

[29] If the rapid azimuthal transport is indeed nearly adiabatic, then energetic particles following non-circular drift orbits should also show day-night differences in the fluxes. Indeed, such differences have already been reported [*Carbary et al.*, 2009; *Paranicas et al.*, 2010; *Kollmann et al.*, 2011]. Using data from the Magnetospheric Imaging Instrument (MIMI) on Cassini [*Krimigis et al.*, 2004], *Carbary et al.* [2009] and *Paranicas et al.* [2010] found a very clear local-time dependence of the energetic electron fluxes (energies ranging from 40 keV to >220 keV) over the radial range from ∼3 to ∼10 Rs, with the highest fluxes

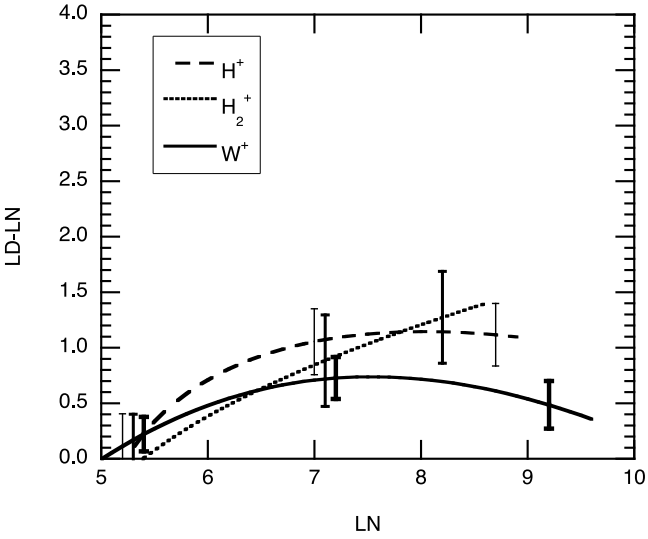

Figure 7. Night-to-day drift path offsets inferred from adiabatic mapping of night-side radial ion temperature profiles to dayside profiles.

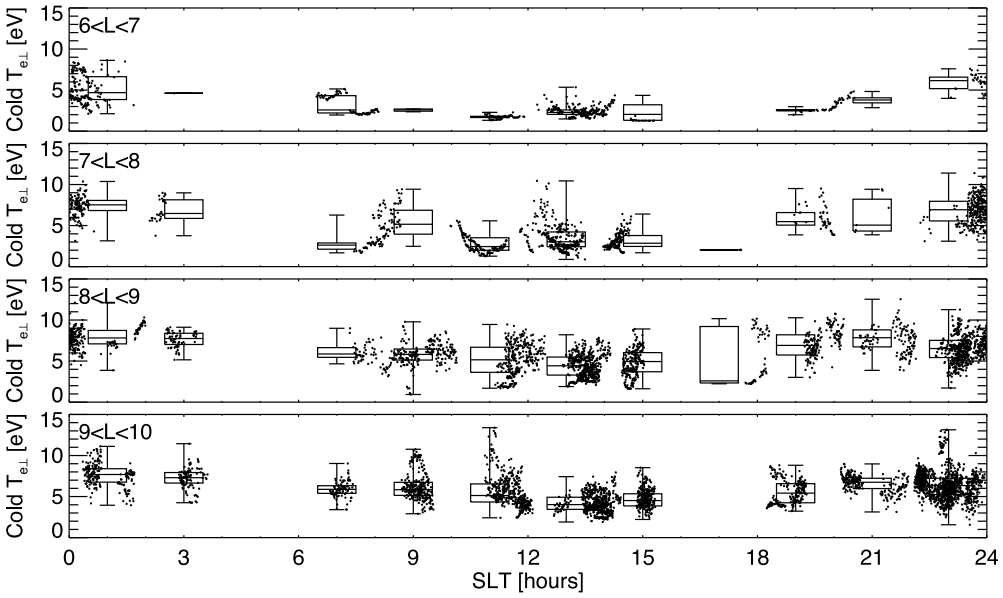

Figure 8. Local time dependence of the cold electron (<150 eV) perpendicular temperature derived from CAPS ELS measurements, for different 1-Rs L bins between L = 6 and L = 10. Solid dots indicate individual 7-min measurements, and boxes indicate the median values in 2-h local time bins.

observed in the midnight region and the lowest ones near noon. In a further analysis of this asymmetry, *Kollmann et al.* [2011] have shown that the day/night asymmetries are also seen in ions with energies ~40 keV. Further, by comparing the radial profiles of fluxes binned by local time (18–06 and 06–18 LT), they showed that the day/night asymmetry in the observed magnetic field strength is far too small to account for the bin differences. They also demonstrated that inside of L~10, there is no discernable dawn/dusk asymmetry in the fluxes.

[30] Under the assumption that these energetic particles also drift essentially adiabatically over the 10 h or so that they take to circle Saturn, Liouville's theorem allows us to estimate the radial offset that would be needed to account for the observed flux differences. Converting the observed fluxes to phase space densities [e.g., *Kollmann et al.*, 2011], we simply find the radial distance on the dayside at which the phase space density has the same value as it has at a given night-side distance, directly yielding the required offset. Figure 11 shows the average phase space densities at constant first and second invariants for both ions and electrons within the MIMI/LEMMS energy range for two local-time bins: 9–15 LT (dayside) and 21–03 LT (night-side). The data cover the time interval from SOI (mid-2004) to early 2011. The filled circles in Figure 11 indicate the night-side data, and the open squares the dayside data. The error bars indicate the standard deviation in the averages and are only shown above each data point since the standard deviations are frequently of the same order as the averages. The data in the figure are plotted on a logarithmic scale, with each tick representing one order of magnitude. The individual curves have arbitrary offsets chosen to enable them all to be displayed in a single figure.

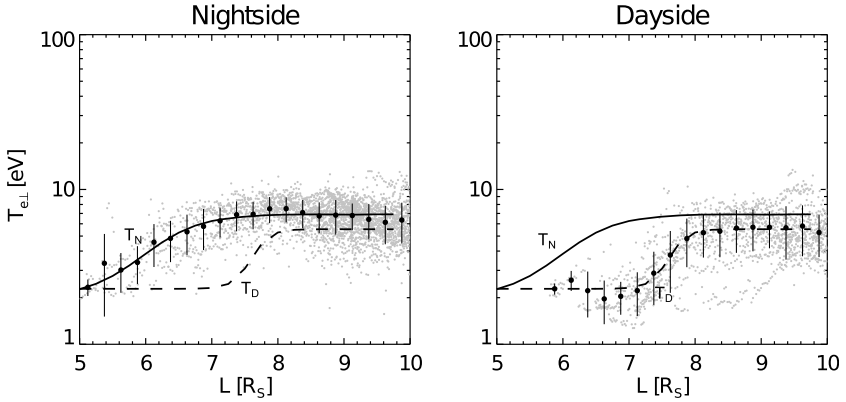

Figure 9. Night-side (21 < LT < 3 h, left) and dayside (9 < LT < 15 h, right) cold electron temperature profiles. Grey dots show individual measurements, solid curves are the night-side tanh fits, and dashed curves are the dayside tanh fits.

Table 2. Parameters for Tanh Fits to Radial Dependence of Cold Electron Temperatures

	a_0 (eV)	a_1 (eV)	a_2 (Rs)	a_3 (Rs)
Day side	3.90969	1.62810	7.65727	0.281881
Night side	4.46304	2.44462	6.21741	0.836222

[31] Figure 11 shows that, although there is significant variability in the fluxes (as indicated by the large error bars), the day/night asymmetry in phase space density profiles is a persistent feature for both electrons and protons, at essentially all values of the first invariant $\mu = \frac{E(E+mc^2)}{2mc^2B}\sin^2\alpha$, where E is the particle kinetic energy, m its rest mass, c the speed of light, and B the magnetic field strength. The profiles in Figure 11 are for a second invariant ($K = \int_{-\lambda_m}^{+\lambda_m} \sqrt{B_m - B}ds$, see *Kollmann et al.* [2011]) of 1.67 $G^{1/2}R_s$, but very similar results are found with other values of K.

[32] Inspection of Figure 11 shows that the day/night offsets between the two phase-space density profiles tend to be of the order of ~1 Rs. To quantify this offset for the full set of first-invariant values, we have fit the dayside and night-side phase-space density profiles in Figure 11 with the following empirically identified function:

$$\log f = aL^2 + bL + c \tag{6}$$

This functional form is not based on any theory; it simply seems to describe the radial dependence of the observed phase-space densities rather well over the full range of mu values.

[33] In analogy to the derivation of equation (2), imposing the requirement that $f_D = f_N$ allows us to solve analytically for the dayside L value corresponding to a given night-side L value:

$$L_D = \frac{-b_D + \sqrt{b_D{}^2 - 4a_D(c_D - F_N)}}{2a_D} \tag{7}$$

where

$$F_N = a_N L_N{}^2 + b_N L_N + c_N$$

Figure 12 shows the resulting offsets L_D-L_N for all of the profiles in Figure 11, except two for which the goodness of the fit to equation (6) was poor (where the correlation coefficient of the fit R < 0.95). For μ_e = 70.00 MeV/G, the analysis yielded negative offsets (see Figure 11), and those are plotted in Figure 12 with the sign reversed and marked with the solid dots. Representative estimates of the

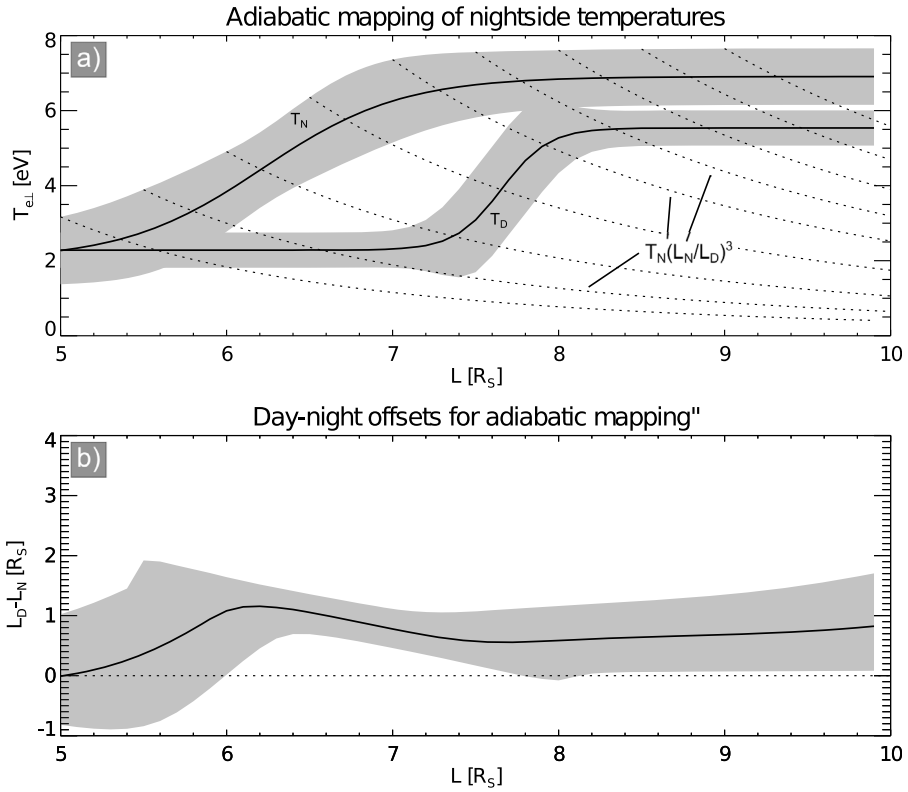

Figure 10. (a) Adiabatic mapping of night-side electron temperature profile (T_N) to the dayside profile (T_D). Dotted curves show the mapped temperature from different night-side locations as a function of day-side distance. The intersections of these curves with the observed dayside profile yield the night-to-day drift offsets. (b) Resulting night-to-day drift offsets for various night-side starting locations. Grey shading shows the uncertainty in the offsets.

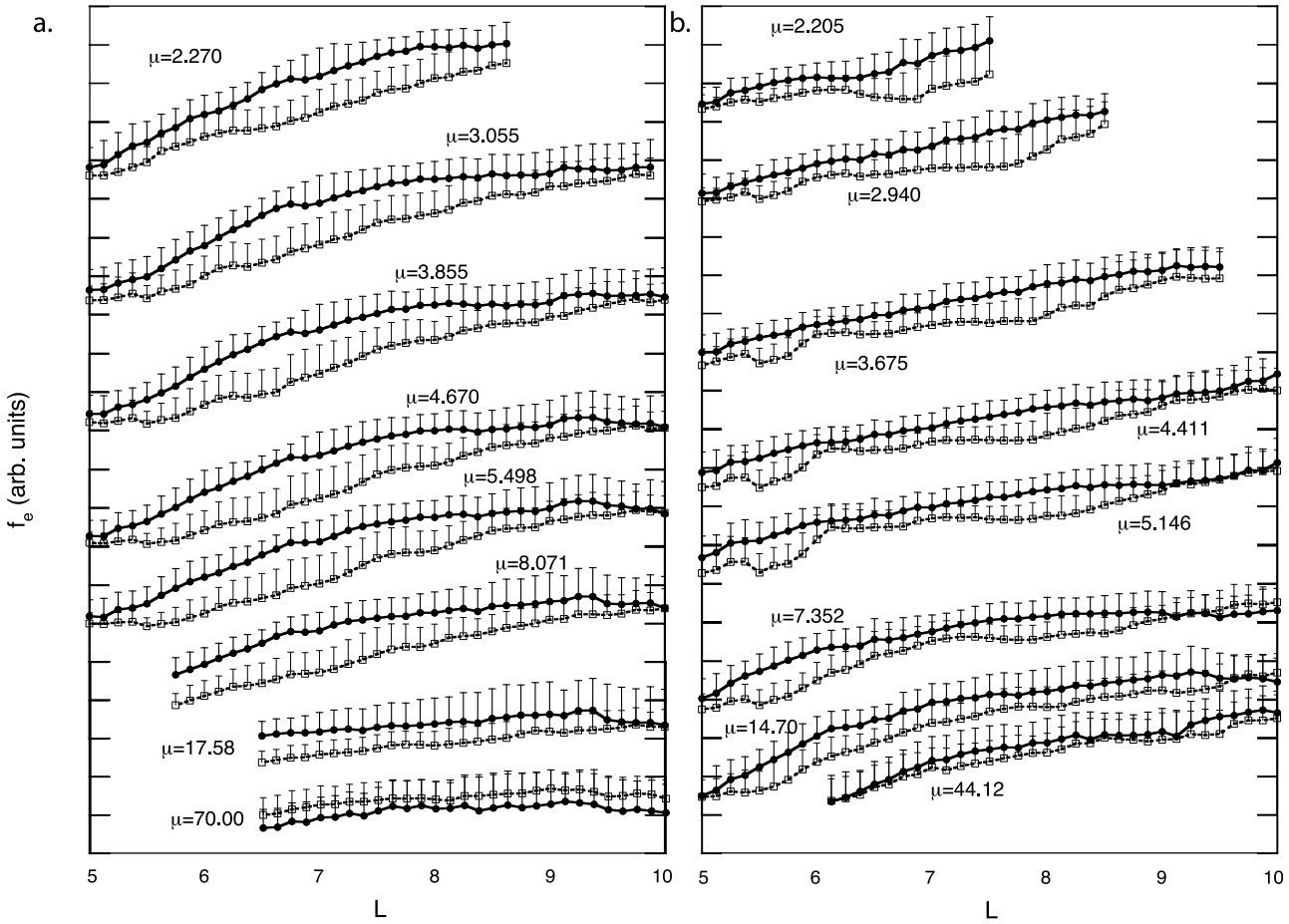

Figure 11. (a) Night-side (filled circles) and dayside (open squares) electron phase space density profiles for a range of first invariants (MeV/G), all for a second invariant of K = 1.67 $G^{1/2}R_s$, corresponding to a pitch angle of 10 degrees at L = 8. The vertical scale is logarithmic, with one decade between ticks and arbitrary offsets to allow all the curves to be plotted in a single frame. (b) Same as Figure 11a for proton phase space densities.

uncertainties, calculated as described above for the ion temperatures, are shown for μ_e = 3.055 MeV/G.

[34] Figure 12 shows that most of the derived offsets tend to turn over and decrease to near zero beyond L∼9.5. While this decline may be real (and does appear to be reflected somewhat in the results for other data sets described above), it may also be at least partly attributable to the fact that the phase-space density plots become much flatter at higher L values, making it difficult to determine the required offset with any precision. The offsets derived for this region represent roughly the lowest values that allow matching of the dayside and nightside fitted curves, but larger values could well be accommodated by the observed phase-space density profiles.

[35] As anticipated above, the offsets in Figure 12 tend to be of the order of 1 Rs, varying somewhat for the different values of μ. There also appears to be a systematic tendency for the offsets derived from proton data (dotted curves in Figure 12) to be somewhat smaller than those derived from electron data (solid curves), as would be expected (c.f., Figure 1). Moreover, careful examination of the color labeling in the figure reveals that there is, with a few exceptions, also a systematic tendency for the offset to increase with increasing electron energies and decrease with increasing proton energies, qualitatively consistent with the expected consequences of the species/energy dependence of the total drift rate. Finally, the fact that the offset for the highest-energy electrons (μ_e = 70.00 MeV/G) was found to be negative is consistent with expectations for particles sufficiently energetic to have a net westward drift, as discussed above.

2.7. SOI Energetic Ion Flux Asymmetry

[36] For exactly the reasons just discussed, the high-energy ions observed in the innermost magnetosphere should also show day-night flux asymmetries. *Paranicas et al.* [2008] showed that the flux profiles of protons with energies greater than ∼12 MeV show remarkable inbound/outbound (i.e., noon/midnight) symmetry in the radial range 2.2 < L < 3.4, with no real discernable difference in the profiles. However, for an electric field of 0.5 mV/m in this region, as inferred by *Paranicas et al.* [2010], the expected day-night offset for the drift paths of such high-energy protons would be less than 0.01 Rs, which would have been difficult to discern in the flux profiles. On the other hand, the expected offset for 2.8 MeV protons would be ∼0.04 Rs, and the inbound/outbound SOI profiles (2.2 < L < 3.3) for

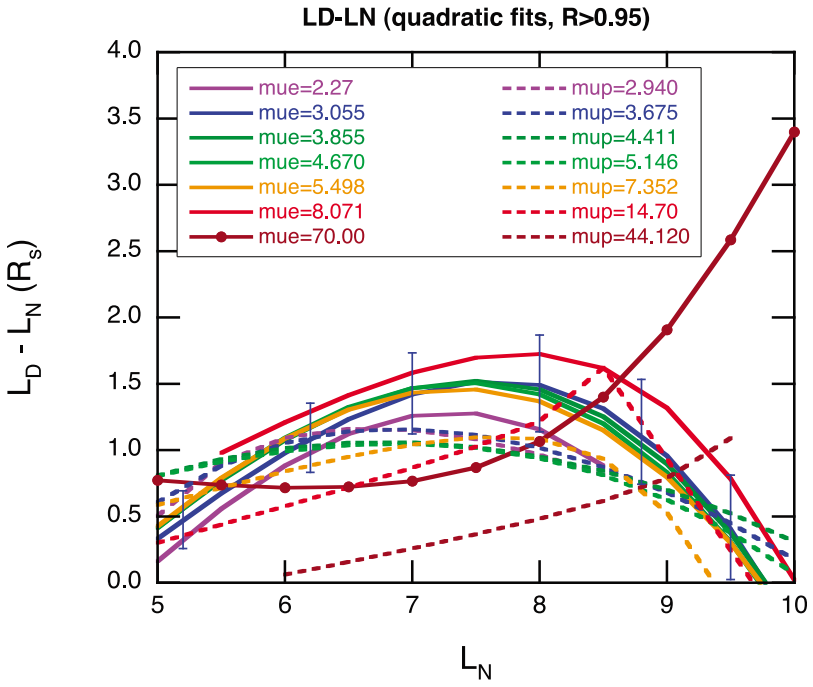

Figure 12. Night-to-day radial drift offsets inferred from adiabatic mapping of phase-space density profiles for various values of the first invariant (MeV/G) and for a second invariant of K = 1.67 $G^{1/2}R_s$. Solid curves correspond to electrons, and dotted curves correspond to protons. The curve marked by solid dots (μ_e = 70.00) actually corresponds to negative values of L_D-L_N, but is shown here with sign reversed. Representative error bars are shown for μ_e = 3.055.

such particles presented in *Paranicas et al.* [2010] are clearly offset by no more than 0.01 Rs. Thus, it appears that the high-energy proton flux profiles for L < 3.4 from SOI are not consistent with the noon-midnight asymmetries expected from a noon-to-midnight electric field of the order of 0.5 mV/m.

3. Discussion

[37] Table 3 summarizes the results of the above comparisons between observations and expectations based on a global dawnward drift due to a noon-to-midnight electric field. Almost all of the observational tests show consistency with the predictions of that hypothesis. The two exceptions are found in observations from the innermost part of the magnetosphere, near the A-ring edge. Thus, we separately address our findings for the regions inside and outside of L∼4.

3.1. L < 4

[38] The inbound/outbound asymmetries in the A-ring absorption signatures of the energetic particles were one of the original pieces of evidence that suggested the existence of a global electric field in the inner magnetosphere, and observations of a similar asymmetry in the total plasma density appear to confirm that conclusion. However, other data reveal several troubling inconsistencies with the interpretation of these offsets:

[39] First, an electric field of this magnitude should yield inbound/outbound offsets in energetic proton flux profiles, whereas no discernable offsets were observed in these channels [*Paranicas et al.*, 2008, 2010].

[40] Second, the LEMMS channel E7, which is believed to count electrons with energies >5 MeV [e.g., *Roussos et al.*, 2007], shows the same in/out offset as the lower-energy channels [*Paranicas et al.*, 2010], contrary to expectations for such high-energy electrons, which should have a net westward drift, leading to an inward displacement on the dayside relative to the night-side location. While there is still some uncertainty as to exactly what energy range is dominating the response of that detector in the inner magnetosphere, it would need to be below 2 or 3 MeV to produce an offset in the observed direction.

Table 3. Consistency of Observations With Expectations for Dawnward Drift

Observation	Consistent	Inconsistent	Comments
Absorption microsignature displacements	X		
A-ring absorption asymmetry SOI (medium-energy particles)	X		
A-ring absorption asymmetry SOI (total electron density)	X		
A-ring absorption asymmetry SOI (high-energy electrons)		X	L∼2.7
Plasma ion temperature asymmetry	X		
Plasma electron temperature asymmetry	X		
Energetic-particle flux asymmetry	X		
Energetic-ion flux asymmetry SOI		X	L < 3.4

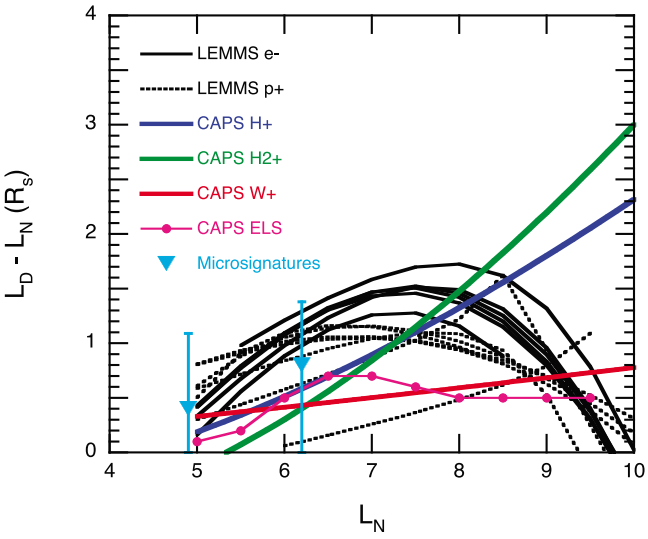

Figure 13. Summary of night-to-day radial drift offsets inferred from five different Cassini data sets. Although there is scatter in the determinations, these independent measurements yield relatively consistent estimates of the offset.

[41] Third, there is a strong pitch angle dependence to the location of the flux drop-off of energetic electrons on the outbound pass at SOI, with the particles near 90-degree pitch angles extending closer to the planet than the field-aligned ones [*Paranicas et al.*, 2010]. This occurs in the region populated by the F-ring and could potentially be attributed to F-ring absorption effects.

[42] Fourth, in our discussion of the expected signatures of a local-time-fixed global convection pattern, we have neglected any discussion of the possible effects of the corotating convection pattern invoked by *Gurnett et al.* [2007] and *Goldreich and Farmer* [2007]. For most of the asymmetries that we have presented, this is valid because the data involve many different passes through the inner magnetosphere at all different SLS longitudes [see, e.g., *Carbary et al.*, 2009], so that longitude-related effects would tend to average out. This is not the case, however, for the SOI observations, which involved only a single inbound and outbound pass. As it turns out, the inbound crossing of the A-ring edge occurred near an SLS2 longitude [*Kurth et al.*, 2007] of 305°, while the outbound crossing occurred near an SLS2 longitude ~244°. According to *Gurnett et al.* [2007], the outflow sector of the postulated corotating convection pattern would be centered near longitude λ_{SLS2}~330°, which is where their measured electron density peaks. Thus, the inbound A-ring crossing, which featured the density drop-off at a radial distance greater than the A-ring edge, would have occurred in the general outflow sector, whereas the outbound crossing would have occurred nearly 90° away from that sector, where the flow in the Gurnett pattern would be mostly azimuthal. However, given that the proposed pattern is so far still a qualitative suggestion, with no quantitative estimate of the strength of the convection, it is not clear at this point whether or not it might explain the observed offsets in the A-ring absorption feature (from lowest to highest energies) or the lack of inbound/outbound flux asymmetries in the energetic protons. We leave this assessment to a future study.

[43] In summary, in light of these inconsistencies, the evidence is not compelling that the inbound/outbound asymmetries observed during SOI in the innermost part of the magnetosphere are attributable to a global local-time-fixed convection pattern. They may arise from asymmetries in the F-ring or possibly from the hypothesized corotating convection pattern [*Gurnett et al.*, 2007; *Goldreich and Farmer*, 2007], but we conclude that they probably have no connection to the day/night asymmetries we have discussed based on observations beyond L~4.

3.2. L > 4

[44] By contrast with the innermost region, all the various lines of evidence for the region beyond L~4 appear to show consistency with the predictions for a global, noon-to-midnight electric field pattern (see Table 3). In Figure 13 we gather all the quantitative estimates of the day-night radial drift offset from the various analyses discussed above. While there is variation in these estimates from data set to data set, they are all of the same sign and generally mutually consistent to within a factor of 2–3.

[45] The most accurate and incontrovertible estimates come from the microsignature displacements. The symbols for those are plotted at the offsets corresponding to the noon extent of the envelope that encompasses most of the observed locations (c.f., Figure 2), while the error bars show the range of the offsets that would arise from the range of electric field values inferred by *Andriopoulou et al.* [2012] (0–0.5 mV/m for Tethys, 0–0.3 mV/m for Dione).

[46] In our discussion of the various curves presented in Figure 13, we have attempted to estimate the uncertainties in the determinations. Sources of those uncertainties include the significant range of values of the various parameters (temperatures and fluxes) about their average values, as well as inaccuracies in the fits to the analytical functions we have chosen to represent the radial profiles of those parameters. As mentioned above, because of large uncertainties in the fits to the H^+ and H_2^+ profiles (probably caused by contamination of the temperatures by hot plasma from interchange events), we have more confidence in values derived from the W^+ temperature asymmetry than in those from either of the light-ion species.

[47] Moreover, it is perhaps not surprising that the different data sets should yield somewhat different offsets since they represent averages over different time intervals and thus magnetospheric conditions and convection strength. Therefore, while Figure 13 shows some variation in the derived offsets, we conclude that they are all generally consistent with average noon-midnight radial drift-path offsets ~0.5–1.5 Rs in the inner magnetosphere outside of L~4. Thus, analysis of these additional data sets supports the conclusions reached by *Roussos et al.* [2005, 2007] and *Andriopoulou et al.* [2012] that the microsignature offsets are best explained by the existence of a global noon-to-midnight electric field with magnitude in the neighborhood of ~0.2 mV/m.

[48] Comparison of Figure 13 with Figure 1 suggests that on the average, the convection electric field strength is probably stronger near L~5 than near L~10. Figure 14 shows the range of electric field values that would

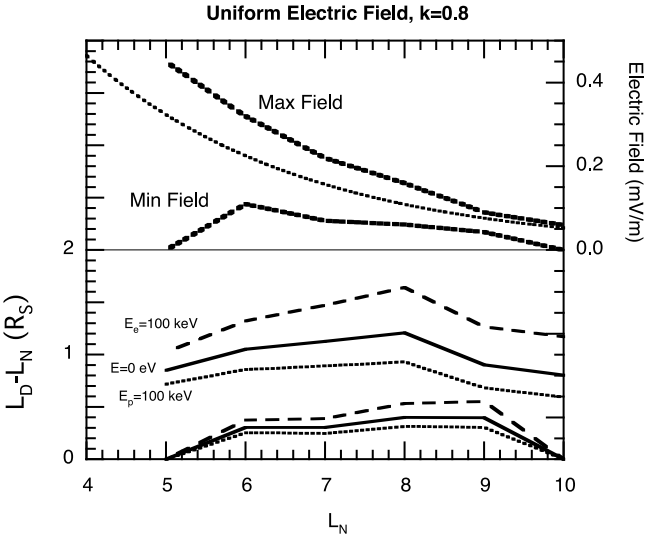

Figure 14. (top) Maximum and minimum noon-to-midnight electric field strengths that would produce radial drift offsets covering the range of inferred values shown in Figure 13. The dotted line shows an exponential curve that roughly splits the range. (bottom) Approximate day-night radial drift offsets that would arise for the maximum and minimum values of the noon-to-midnight convection electric field shown in the upper half of the figure. The top three curves in the bottom of the figure are the offsets that correspond to the maximum field strength, and the lower three curves are those corresponding to the minimum field strength. The long-dashed curves show the offsets for electrons with energies of 100 keV, while the solid curves are for zero-energy particles, and the dotted curves are for ions with energies of 100 keV.

reproduce the general range of radial drift-path offsets that we have inferred (Figure 13). For the min-max range of field strengths shown in the upper half of the figure by the heavy dashed lines, the curves in the lower half of the figure show the resulting radial offsets, with the upper three corresponding to the maximum-field-strength curve and the lower three corresponding to the minimum field strength. As in Figure 1, the long-dashed lines are for electrons with energy of 100 keV, the solid lines are for zero-energy particles, and the dotted lines are for protons with energy of 100 keV.

3.3. Drift Velocities

[49] If the field strength does depend on L, as suggested by Figures 13 and 14, then a uniform noon-to-midnight electric field is not the correct description of the global convection pattern we are investigating, and the calculations shown in Figures 1 and 14 (as well as those used by previous authors) are not strictly correct since they assume that the field has a constant value over the entire drift orbit, even though L differs from L_N over the course of the drift. Nonetheless, while the actual spatial configuration of this convection pattern is beyond the scope of the present work, it is useful to use the uniform-field approximation to estimate the magnitude of the plasma drift velocities in both the magnetosphere and the ionosphere that would correspond to field strengths inferred within that approximation (e.g., Figure 14).

[50] Figure 15 shows the average magnetospheric drift velocities in the radial and azimuthal direction that would result from a "uniform" noon-to-midnight electric field with a magnitude as shown by the dotted line in the top half of Figure 14, which more or less splits the range between the maximum and minimum field values shown there. The inferred drift velocities are well within the limits reported from CAPS measurements by *Sittler et al.* [2006] and *Wilson et al.* [2008] and range from ~3–4% of corotation. Figure 16 shows the corresponding average drift velocities in the northern ionosphere, where we have mapped the velocities assuming the dipolar field lines are equipotentials:

$$V_{I\theta} = \frac{-V_{Mr}}{2L(L-1)^{1/2}} \tag{8}$$

$$V_{I\varphi} = \frac{V_{M\varphi}}{L^{3/2}} \tag{9}$$

$V_{I\theta}$ is negative for poleward flows in the northern hemisphere and would be the opposite in the southern hemisphere. The required azimuthal flows in the ionosphere are at most a few percent of the atmospheric rotation rate, and the polar flows are even smaller.

3.4. Alternative Explanations of Day/Night Asymmetries

[51] Previous authors [e.g., *Carbary et al.*, 2009; *Paranicas et al.*, 2010; *Kollmann et al.*, 2011; *DeJong et al.*, 2011] have proposed an alternate explanation for the day/night energetic-particle flux asymmetries (e.g., Figure 11) in terms of a higher likelihood of particle injections (or interchange events) on the nightside, followed by drift dispersion and various losses as particles drift to the day side. While observations do suggest that energetic particle injections occur more frequently in the night and morning sectors (21–09 LT) [*Müller et al.*, 2010], the local time distribution for interchange events peaks primarily in the dawn sector (04–12 LT) [*Chen and Hill*, 2008]. In addition, the dispersion and loss scenario would also predict higher fluxes at dawn than at dusk, which is not observed [*Kollmann et al.*, 2011]. The symmetry of energetic particle fluxes around local noon [e.g., *Carbary et al.*, 2009; *Paranicas et al.*, 2010; *Kollmann et al.*, 2011] argues instead for an adiabatic (i.e., reversible) reduction in fluxes as particles drift to the dayside, with the reduction reversed during the subsequent return to the night side. A noon-to-midnight electric field would produce precisely that effect.

[52] Furthermore, the radial offsets observed in the satellite microsignatures [*Andriopoulou et al.*, 2012] are particularly strong evidence that net outward drifts from the night side to the day side and net inward drifts from the day side to the night side do occur.

3.5. Origin of the Electric Field

[53] The origin of a noon-to-midnight convection electric field that could give rise to the noncircular drift orbits inferred in this study and previous ones is not clear. As noted earlier, transfer of the solar wind electric field into the

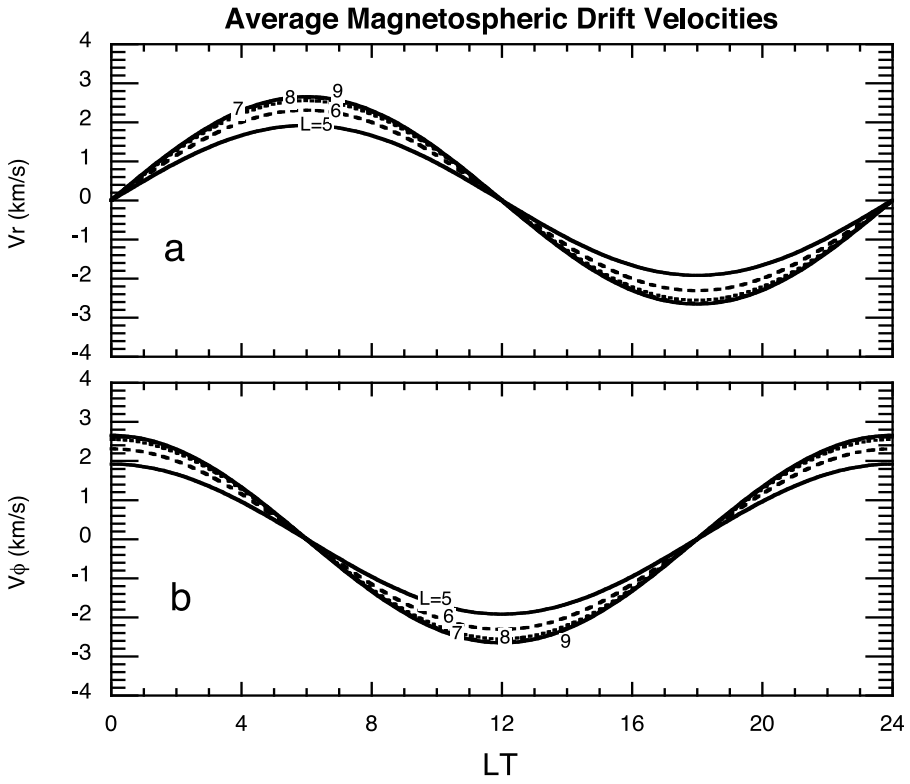

Figure 15. Average drift velocities in the (top) radial and (bottom) azimuthal directions for a noon-to-midnight electric field with the radial dependence shown as the dotted curve in the upper half of Figure 14.

magnetosphere is not a likely candidate, both because of the larger magnitude and the different orientation compared to what would be expected of that mechanism [e.g., *Cooper et al.*, 1998]. Moreover, Figure 14 suggests that the strength of the convection field actually increases with decreasing L, contrary to what one would expect from a convection pattern imposed from the solar wind. This L dependence would seem to argue for convection that is imposed internal to the magnetosphere.

[54] One possibility is that it may be due to diurnally varying neutral winds driven by subsolar heating. The atmospheric circulation driven by solar EUV heating has been modeled by *Müller-Wodarg et al.* [2006], who find that solar heating produces horizontal winds of less than 20 m/s, dominantly in the zonal direction due to strong Coriolis forces on poleward-expanding flows. Not only are such flows significantly smaller than the ionospheric velocities inferred here, but for equinox conditions the model shows the strongest poleward flows in the 12–24 LT region in the range of $L > 5$, the opposite of what we infer (Figure 16). For solstice conditions, the model shows weak meridional flows away from the sunlit pole at essentially all local times, also inconsistent with the pattern we infer. In addition to the solar EUV heating, *Müller-Wodarg et al.* [2006] have evaluated the effect on atmospheric circulation of Joule heating due to auroral energy deposition above ~70 degrees latitude (L~9). They found auroral heating to be a much stronger driver of atmospheric circulation than solar heating, with zonal flows up to ~3 km/s at 60 degrees latitude (L~4) and persisting at ~100 s of m/s to low and high latitudes ($3 < L < 10$). The meridional winds were equatorward and peaked near 300 m/s at ~50 degrees latitude (L~2.4). Their model assumed energy deposition that was independent of local time, so their results are diurnally averaged. However, ultraviolet images show that the aurorae are frequently brightest on the dawn side [e.g., *Clarke et al.*, 2005], and if we assume that the auroral energy deposition is greatest at dawn, the modeling of *Müller-Wodarg et al.* [2006] might suggest that we would expect to see equatorward flows dominantly in the dawn sector. This, unfortunately, is the opposite of the direction required to explain the noon bulge in the drift orbits inferred in the present study.

[55] To explain a dawn-dusk asymmetry in the UV emission from the Io plasma torus observed by the Voyager UVS instrument [*Shemansky and Sandel*, 1982], *Barbosa and Kivelson* [1983] and *Ip and Goertz* [1983] independently invoked a dawn-to-dusk convection electric field in the inner Jovian magnetosphere, which would cause noncircular drift orbits that are closer to Jupiter at dusk than at dawn. Exactly as described above in our discussion of the day-night asymmetry of the plasma ion and electron temperature, the electron population responsible for the UV emissions would alternately be heated and cooled adiabatically as it drifted on the noncircular trajectories, providing greater energy input at dusk than at dawn. *Barbosa and Kivelson* [1983] found that a convection field ~4 mV/m (3% of the corotation field) would be required to produce the inferred dawn-dusk temperature difference, and *Ip and Goertz* [1983] derived a value of 1.6 mV/m. These values are very much greater than the dusk-to-dawn field expected from solar wind-driven convection [*Barbosa and Kivelson*, 1983], and the dawn-to-dusk direction is moreover opposite to that expected from

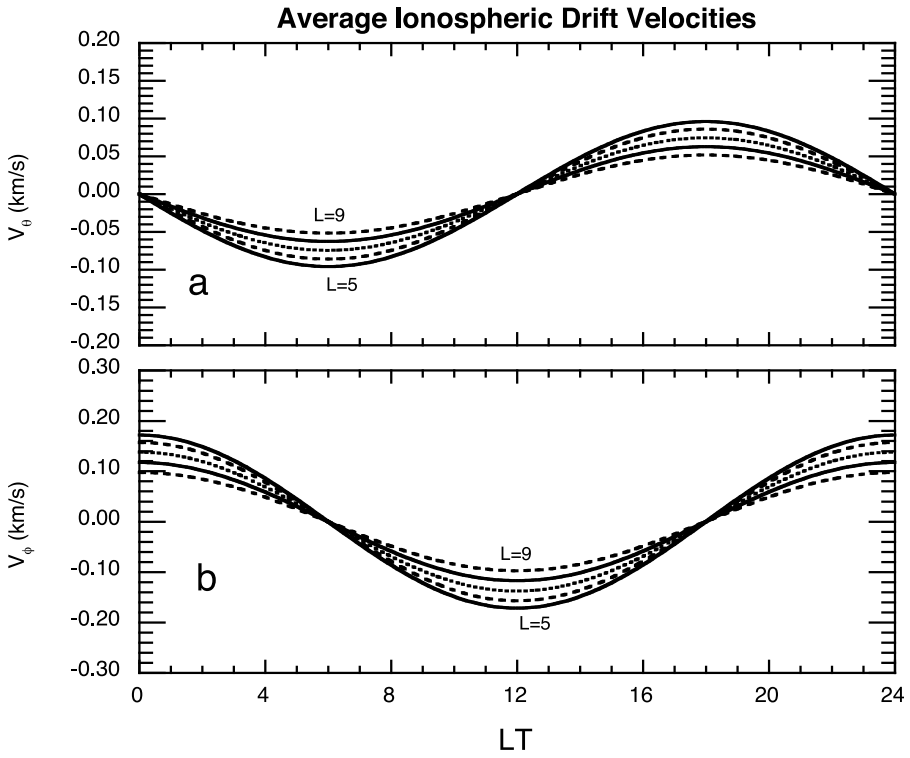

Figure 16. Average drift velocities in the ionosphere, mapped from the magnetospheric velocities shown in Figure 15. (a) The meridional component; (b) the zonal component.

the solar wind influence [*Ip and Goertz*, 1983]. Consequently, both of these papers attributed this electric field to the tailward escape of magnetospheric plasma (the "planetary wind").

[56] The physics of this planetary-wind-driven electric field was explored in some detail by *Goertz and Ip* [1984]. Qualitatively, they argued that the loss of plasma down the tail of Jupiter's magnetosphere created a low-density region outside of a higher-density region in which plasma could still execute closed drift orbits. The distortion of the boundary between low- and high-density regions relative to paths of centrifugal drift current results in a current divergence in the equatorial plane, which must be closed through Birkeland currents out of the ionosphere on the dusk side and into the ionosphere on the dawn side. Ionospheric closure of this current then requires a dawn-to-dusk electric field in the ionosphere, which in turn maps out into the magnetosphere. With detailed calculations, *Goertz and Ip* [1984] estimated a dawn-dusk potential difference across the orbit of Io of >1 MV, which compared favorably with the potential difference of 1.3 MV that would be produced by a uniform field of 1.5 mV/m. They further argued that a similar situation would probably be expected at Saturn, which is similarly subject to downtail plasma losses due to the strong centrifugal forces on rapidly corotating plasma. However, if this mechanism is to explain the noon-to-midnight electric field we have inferred in this study, it would require that the current system envisioned by *Goertz and Ip* [1984] would need to be rotated nearly 90 degrees in local time, such that the Birkeland currents are out of the ionosphere on the night side of the magnetosphere and into the ionosphere on the dayside. The cause of such a rotation is not immediately obvious, so we leave investigation of this possibility for future work.

[57] Thus, the cause of the inferred noon-to-midnight electric field remains a puzzle. Whatever the cause of this field, however, it appears to be a dominant factor in the circulation of charged particles in Saturn's inner magnetosphere ($5 < L < 10$).

4. Summary

[58] In this study we have presented several lines of observational evidence to test the proposal that there exists a local-time-fixed convection pattern in Saturn's inner magnetosphere [e.g., *Roussos et al.*, 2005, 2007; *Andriopoulou et al.*, 2012]. These include a) day/night asymmetries in the A-ring absorption signature of both high-energy particles and total electron density, b) day/night asymmetries in plasma ion and electron temperatures, and c) day/night asymmetries in energetic-particle phase-space densities. Beyond L∼4, the observations are found to be consistent with expectations based on the suggested global convection pattern. The various lines of evidence yield relatively consistent estimates for typical day-night radial drift offsets of ∼0.5–1 Rs. The noon-to-midnight electric field that would be needed to produce such drift-orbit displacements is consistent with those reported in earlier studies. The necessary electric field strength appears to decrease with radial distance, from ∼0.3 mV/m near Tethys to <0.1 mV/m near L = 10. Corresponding average drift velocities attributable to such an electric field are a few km/s in both the radial and azimuthal direction, mapping to ionospheric velocities up to 200 m/s. The source for a noon-to-midnight electric field at

Saturn is not obvious, and to date we do not have a good explanation for it. The magnitude, direction, and radial dependence all argue against production via coupling to the solar wind electric field, but no very plausible internal sources have emerged either. It may be that the field is somehow associated with Saturn's planetary wind, as discussed for Jupiter by *Barbosa and Kivelson* [1983], *Ip and Goertz* [1983], and *Goertz and Ip* [1984], but that mechanism would require a 90-degree rotation to produce the observed offsets. Thus, for now the source of the convection field remains a puzzle. For $L < 4$, the observations are not fully consistent with such a global convection field, and other explanations for A-ring absorption asymmetries are needed.

[59] **Acknowledgments.** The authors are grateful to our many colleagues on the various Cassini instrument teams for making the present study possible. Thanks to G. R. Lewis and L. K. Gilbert for ELS data processing. Work at Los Alamos was conducted under the auspices of the U.S. Department of Energy, with support from the NASA Cassini program. C.S.A. was supported by an STFC postdoctoral fellowship. The Cassini Plasma Spectrometer was supported by JPL contract 1243218 with Southwest Research Institute. The Cassini project is managed by the Jet Propulsion Laboratory for NASA.

[60] Masaki Fujimoto thanks Atsuhiro Nishida and another reviewer for their assistance in evaluating this paper.

References

Andriopoulou, M., E. Roussos, N. Krupp, C. Paranicas, M. Thomsen, S. Krimigis, M. K. Dougherty, and K.-H. Glassmeier (2012), A noon-to-midnight electric field and nightside dynamics in Saturn's inner magnetosphere, using microsignature displacements, *Icarus*, *220*, 503.

Arridge, C. S., L. K. Gilbert, G. R. Lewis, E. C. Sittler, G. H. Jones, D. O. Kataria, A. J. Coates, and D. T. Young (2009), The effect of spacecraft radiation sources on electron moments from the Cassini CAPS Electron Spectrometer, *Planet. Space Sci.*, *57*(7), 854, doi:10.1016/j.pss.2009.02.011.

Barbosa, D. D., and M. G. Kivelson (1983), Dawn-dusk electric field asymmetry of the Io plasma torus, *Geophys. Res. Lett.*, *10*(3), 210, doi:10.1029/GL010i003p00210.

Burch, J. L., J. Goldstein, T. W. Hill, D. T. Young, F. J. Crary, A. J. Coates, N. André, W. S. Kurth, and E. C. Sittler Jr. (2005), Properties of local plasma injections in Saturn's magnetosphere, *Geophys. Res. Lett.*, *32*, L14S02, doi:10.1029/2005GL022611.

Carbary, J. F., D. G. Mitchell, N. Krupp, and S. M. Krimigis (2009), L shell distribution of energetic electrons at Saturn, *J. Geophys. Res.*, *114*, A09210, doi:10.1029/2009JA014341.

Chen, Y., and T. W. Hill (2008), Statistical analysis of injection/dispersion events in Saturn's inner magnetosphere, *J. Geophys. Res.*, *113*, A07215, doi:10.1029/2008JA013166.

Chen, Y., T. W. Hill, A. M. Rymer, and R. J. Wilson (2010), Rate of radial transport of plasma in Saturn's inner magnetosphere, *J. Geophys. Res.*, *115*, A10211, doi:10.1029/2010JA015412.

Clarke, J. T., et al. (2005), Morphological differences between Saturn's ultraviolet aurorae and those of Earth and Jupiter, *Nature*, *433*, 717, doi:10.1038/nature03331.

Cooper, J. F., E. C. Sittler Jr., S. Maurice, B. H. Mauk, and R. S. Selesnick (1998), Local time asymmetry of drift shells for energetic electrons in the middle magnetosphere of Saturn, *Adv. Space Res.*, *21*, 1479, doi:10.1016/S0273-1177(98)00022-2.

DeJong, A. D., J. L. Burch, J. Goldstein, A. J. Coates, and F. Crary (2011), Day-night asymmetries of low-energy electrons in Saturn's inner magnetosphere, *Geophys. Res. Lett.*, *38*, L08106, doi:10.1029/2011GL047308.

Goertz, C. K., and W.-H. Ip (1984), A dawn-to-dusk electric field in the Jovian magnetosphere, *Planet. Space Sci.*, *32*, 179, doi:10.1016/0032-0633(84)90152-1.

Goldreich, P., and A. J. Farmer (2007), Spontaneous axisymmetry breaking of the external magnetic field at Saturn, *J. Geophys. Res.*, *112*, A05225, doi:10.1029/2006JA012163.

Gurnett, D. A., et al. (2004), The Cassini radio and plasma wave investigation, *Space Sci. Rev.*, *114*, 395, doi:10.1007/s11214-004-1434-0.

Gurnett, D. A., et al. (2005), Radio and plasma wave observations at Saturn from Cassini's approach and first orbit, *Science*, *307*, 1255, doi:10.1126/science.1105356.

Gurnett, D. A., et al. (2007), The variable rotation period of the inner region of Saturn's plasma disk, *Science*, *316*, 442, doi:10.1126/science.1138562.

Hansen, C. J., L. Esposito, A. I. F. Stewart, J. Colwell, A. Hendrix, W. Pryor, D. Shemansky, and R. West (2006), Enceladus' water vapor plume, *Science*, *311*, 1422, doi:10.1126/science.1121254.

Hill, T. W. (1979), Inertial limit on corotation, *J. Geophys. Res.*, *84*, 6554, doi:10.1029/JA084iA11p06554.

Hill, T. W., A. M. Rymer, J. L. Burch, F. J. Crary, D. T. Young, M. F. Thomsen, D. Delapp, N. André, A. J. Coates, and G. R. Lewis (2005), Evidence for rotationally driven plasma transport in Saturn's magnetosphere, *Geophys. Res. Lett.*, *32*, L14S10, doi:10.1029/2005GL022620.

Hill, T. W., et al. (2008), Plasmoids in Saturn's magnetotail, *J. Geophys. Res.*, *113*, A01214, doi:10.1029/2007JA012626.

Ip, W.-H., and C. K. Goertz (1983), An interpretation of the dawn-dusk asymmetry of UV emission from the Io plasma torus, *Nature*, *302*, 232, doi:10.1038/302232a0.

Jackman, C. M., C. T. Russell, D. J. Southwood, C. S. Arridge, N. Achilleos, and M. K. Dougherty (2007), Strong rapid dipolarizations in Saturn's magnetotail: In situ evidence of reconnection, *Geophys. Res. Lett.*, *34*, L11203, doi:10.1029/2007GL029764.

Kollmann, P., E. Roussos, C. Paranicas, N. Krupp, C. M. Jackman, E. Kirsch, and K.-H. Glassmeier (2011), Energetic particle phase space densities at Saturn: Cassini observations and interpretations, *J. Geophys. Res.*, *116*, A05222, doi:10.1029/2010JA016221.

Krimigis, S. M., et al. (2004), Magnetospheric Imaging Instrument (MIMI) on the Cassini Mission to Saturn/Titan, *Space Sci. Rev.*, *114*, 233, doi:10.1007/s11214-004-1410-8.

Kurth, W. S., A. Lecacheux, T. F. Averkamp, J. B. Groene, and D. A. Gurnett (2007), A Saturnian longitude system based on a variable kilometric radiation period, *Geophys. Res. Lett.*, *34*, L02201, doi:10.1029/2006GL028336.

Lewis, G. R., N. André, C. S. Arridge, A. J. Coates, L. K. Gilbert, D. R. Linder, and A. M. Rymer (2008), Derivation of density and temperature from the Cassini-Huygens CAPS Electron Spectrometer, *Planet. Space Sci.*, *56*(7), 901, doi:10.1016/j.pss.2007.12.017.

Müller, A. L., J. Saur, N. Krupp, E. Roussos, B. H. Mauk, A. M. Rymer, D. G. Mitchell, and S. M. Krimigis (2010), Azimuthal plasma flow in the Kronian magnetosphere, *J. Geophys. Res.*, *115*, A08203, doi:10.1029/2009JA015122.

Müller-Wodarg, I. C. F., M. Mendillo, R. V. Yelle, and A. D. Aylward (2006), A global circulation model of Saturn's thermosphere, *Icarus*, *180*, 147, doi:10.1016/j.icarus.2005.09.002.

Paranicas, C., D. G. Mitchell, S. Livi, S. M. Krimigis, E. Roussos, N. Krupp, J. Woch, A. Lagg, J. Saur, and F. S. Turner (2005), Evidence of Enceladus and Tethys microsignatures, *Geophys. Res. Lett.*, *32*, L20101, doi:10.1029/2005GL024072.

Paranicas, C., D. G. Mitchell, S. M. Krimigis, D. C. Hamilton, E. Roussos, N. Krupp, G. H. Jones, R. E. Johnson, J. F. Cooper, and T. P. Armstrong (2008), Sources and losses of energetic protons in Saturn's magnetosphere, *Icarus*, *197*, 519, doi:10.1016/j.icarus.2008.05.011.

Paranicas, C., et al. (2010), Asymmetries in Saturn's radiation belts, *J. Geophys. Res.*, *115*, A07216, doi:10.1029/2009JA014971.

Press, W. H., S. A. Teukolsky, W. T. Vetterling, and B. P. Flannery (2001), *Numerical Recipes in Fortran 77: The Art of Scientific Computing*, vol. 1, 2nd ed., Cambridge Univ. Press, New York.

Richardson, J. D. (1986), Thermal ions at Saturn: Plasma parameters and implications, *J. Geophys. Res.*, *91*, 1381, doi:10.1029/JA091iA02p01381.

Roussos, E., et al. (2005), Low energy electron microsignatures at the orbit of Tethys: Cassini MIMI/LEMMS observations, *Geophys. Res. Lett.*, *32*, L24107, doi:10.1029/2005GL024084.

Roussos, E., G. H. Jones, N. Krupp, C. Paranicas, D. G. Mitchell, A. Lagg, J. Woch, U. Motschmann, S. M. Krimigis, and M. K. Dougherty (2007), Electron microdiffusion in the Saturnian radiation belts: Cassini MIMI/LEMMS observations of energetic electron absorption by the icy moons, *J. Geophys. Res.*, *112*, A06214, doi:10.1029/2006JA012027.

Rymer, A. M., et al. (2007), Electron sources in Saturn's magnetosphere, *J. Geophys. Res.*, *112*, A02201, doi:10.1029/2006JA012017.

Shemansky, D. E., and B. R. Sandel (1982), The injection of energy into the Io plasma torus, *J. Geophys. Res.*, *87*, 219, doi:10.1029/JA087iA01p00219.

Sittler, E. C., et al. (2006), Cassini observations of Saturn's inner plasmasphere: Saturn orbit insertion results, *Planet. Space Sci.*, *54*, 1197, doi:10.1016/j.pss.2006.05.038.

Sittler, E. C., et al. (2008), Ion and neutral sources and sinks within Saturn's inner magnetosphere: Cassini results, *Planet. Space Sci.*, *56*, 3, doi:10.1016/j.pss.2007.06.006.

Spitale, J. N., and C. C. Porco (2009), Time variability in the outer edge of Saturn's A-ring revealed by Cassini imaging, *Astron. J.*, *138*, 1520, doi:10.1088/0004-6256/138/5/1520.

Thomsen, M. F., and J. A. Van Allen (1980), Motion of trapped electrons and protons in Saturn's inner magnetosphere, *J. Geophys. Res.*, *85*, 5831, doi:10.1029/JA085iA11p05831.

Thomsen, M. F., D. B. Reisenfeld, D. M. Delapp, R. L. Tokar, D. T. Young, F. J. Crary, E. C. Sittler, M. A. McGraw, and J. D. Williams (2010), Survey of ion plasma parameters in Saturn's magnetosphere, *J. Geophys. Res.*, *115*, A10220, doi:10.1029/2010JA015267.

Waite, J. H., et al. (2006), Cassini ion and neutral mass spectrometer: Enceladus plume composition and structure, *Science*, *311*, 1419, doi:10.1126/science.1121290.

Wilson, R. J., R. L. Tokar, M. G. Henderson, T. W. Hill, M. F. Thomsen, and D. H. Pontius Jr. (2008), Cassini plasma spectrometer thermal ion measurements in Saturn's inner magnetosphere, *J. Geophys. Res.*, *113*, A12218, doi:10.1029/2008JA013486.

Young, D. T., et al. (2004), Cassini Plasma Spectrometer investigation, *Space Sci. Rev.*, *114*, 1, doi:10.1007/s11214-004-1406-4.